INT. J. GEOGRAPHICAL INFORMATION SCIENCE, 1998, VOL. 12, NO. 8, 805–827

Research Article

Comparing area and shape distortion on polyhedral-based recursive partitions of the sphere

DENIS WHITE†, A. JON KIMERLING, KEVIN SAHR and LIAN SONG

Department of Geosciences, Oregon State University, Corvallis, OR 97331, USA
e-mail: denis@mail.cor.epa.gov

(*Received 10 December 1996; accepted 27 February 1998*)

Abstract. Regular grid sampling structures in the plane are a common spatial framework for many studies. Constructing grids with desirable properties such as equality of area and shape is more difficult on a sphere. We studied the distortion characteristics of recursive partitions of the surface of the globe starting with the octahedron and icosahedron polyhedral models. We used five different methods for mapping from the polyhedral model to the surface of the sphere: the Gnomonic projection, Fuller's Dymaxion projection, Snyder's equal area polyhedral projection, direct spherical subdivision, and a recursive polyhedral projection. We increased partition density using both a 4-fold and a 9-fold ratio at each level of recursive subdivision by subdividing to the 8th level with the 4-fold density ratio (65 536 cells per polyhedral face) and to the fifth level with the 9-fold density ratio (59 049 cells per polyhedral face). We measured the area and perimeter of each cell at each level of recursion for each method on each model using each density ratio. From these basic measurements we calculated the range and standard deviation of the area measurement, and the mean, range, and standard deviation of a compactness measurement defined as the ratio of (the ratio of the perimeter to the area of the cell) to (the ratio of the perimeter to the area of a spherical circle with the same area). We looked at these basic measurements and their statistics using graphs of variation with recursion level, sums of squares analyses of variation, histograms of the distributions, maps of the spatial variation, and correlograms. The Snyder projection performed best in area distortion and the Gnomonic projection performed best in compactness distortion. The Fuller projection and the Sphere method had moderate distortion in both area and compactness relative to the worst methods. There was little difference in distortion performance between partitions using the 4-fold density ratio and those using the 9-fold density ratio. Partitions based on the icosahedron performed better for all statistics than those based on the octahedron.

1. Introduction

Global change studies often need an assumption-free method for partitioning the earth or some subset of it into sampling or analysis units. Rather than adopting a geographical framework based on political divisions, or on scientific criteria that may be different from those of the study at hand, investigators often choose to

† Author's present address: US EPA, 200 SW 35th St., Corvallis, OR 97333, USA.

1365-8816/98 $12.00

impose a regular geometric grid that is unbiased with respect to patterns that arbitrary natural processes or human institutions may have created.

For studies in small areas over which distortions due to the curvature of the earth are negligible, it is easy to create such a grid by assuming that the study area can be represented on a plane. On a sphere, or nearly spherical surface such as the Earth, it is more difficult. We began investigating the construction of equal area partitions of the globe in our earlier work (White *et al.* 1992). This work was based on the truncated icosahedron positioned on the Earth to optimally cover the conterminous US in one hexagon face of the model projected to the sphere, followed by a triangular grid of points with a corresponding tessellation of hexagons at different densities developed upon the planar hexagon face. Weaknesses of the initial approach included (1) the use of the Lambert equal area azimuthal projection that did not project exactly from a hexagon face of the truncated icosahedron to the corresponding spherical hexagon, leaving sliver areas along the edges, (2) the difficulty of extending grid networks over the pentagon faces of the truncated icosahedron model, (3) a mixed-factor hierarchy of grid densities that was designed to allow more choice in sampling density but complicated the generation of custom grids, (4) a lack of computer data structure or database management system, and (5) the bias in the positioning of the grid to optimize for one country. To address some of these weaknesses, we initiated a more comprehensive study of global grid systems and the geometric distortions that they create.

In this paper, we present a systematic study of a class of global partitions based on recursive subdivisions of the faces of the octahedron and icosahedron. Our objectives were to compare the distortion performance of partitions along four different dimensions of variation, or factors. The first factor was the initial geometric model, either octahedron or icosahedron. The second factor was the method for mapping the surface of the geometric model to the surface of the sphere. The third factor was the change in density of the partition between levels of recursion. The final factor was level of recursion, which corresponds to size of grid as measured by, for example, number of cells.

2. Methods of partition

The framework for our study was the subdivision of the surface of the Earth using regular polyhedra as initial models. These polyhedral-based partitions are only one of several classes of methods for developing global grids (White *et al.* 1992). In this study we investigated partitions based on the triangular faces of an octahedron and an icosahedron. We selected the icosahedron because it is the highest order regular three-dimensional polyhedron in number of faces. We hypothesized that this model would therefore produce partitions with less distortion than those based on the other regular polyhedra. We selected the octahedron as a model for comparison for two reasons. First, several proposed global grid systems use the octahedron (Dutton 1988, Goodchild and Yang 1992, Lugo and Clarke 1995, Dutton 1996). Second, it is the next highest order regular polyhedron having triangular faces, therefore it is straightforward to compare with the icosahedron. A different standard of comparison would be necessary to compare the triangular faces of the icosahedron with the pentagonal faces of the dodecahedron or the square faces of the hexahedron.

Within a triangular face of either the icosahedron or the octahedron, we implemented a recursive partitioning process, using either a 4-fold or a 9-fold increase in density of cells at each level of recursion (figure 1). These two methods of recursive

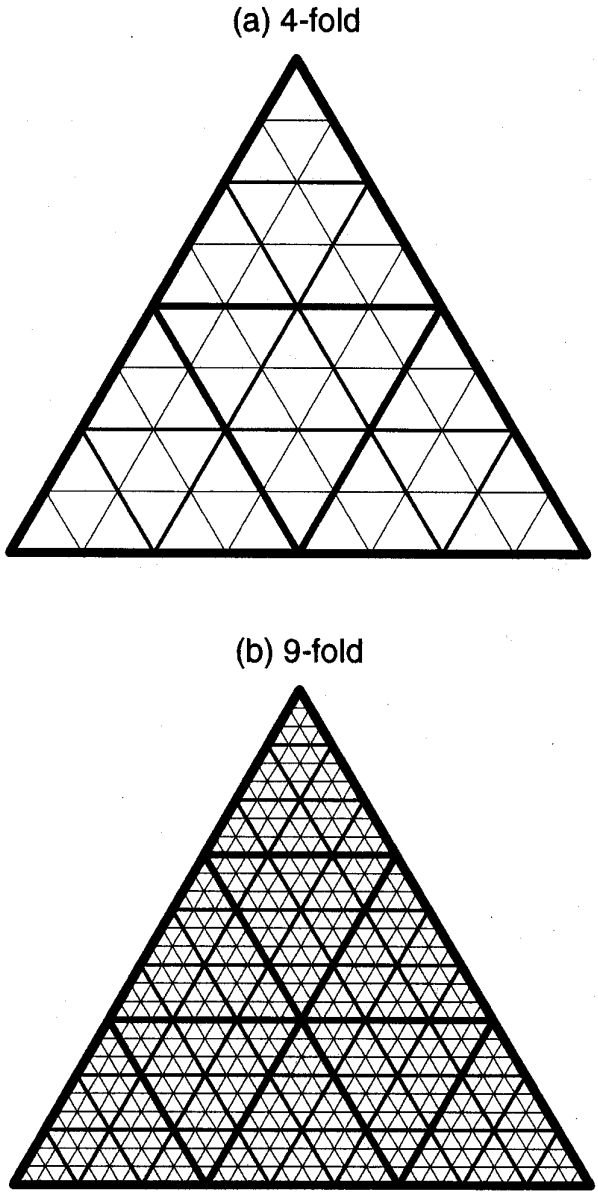

Figure 1. Recursive partitioning of a triangular face of the icosahedron (or octahedron): (*a*) using the 2-frequency subdivision of edges and the 4-fold density ratio; (*b*) using the 3-frequency subdivision of edges and the 9-fold density ratio. The first three recursion levels are shown.

partitioning are sometimes called the 2-frequency and 3-frequency cases (Popko 1968) because the partitions are created by subdividing each edge of the triangle into two or three equal segments, respectively, and connecting the nearest neighbour segment endpoints to create the next level partition.

Each of the two density-changing methods has advantages. Although all analyses in this paper were performed on the triangular cells of the partitions, for the purpose of discussing the comparative advantages of the two density factors, we focus on the hexagon tessellations induced by the 4-fold and 9-fold partitions (figure 2), since for many applications the more compact shape of hexagons will be preferred as the cell structure rather than that of the triangles. (In a related paper (Kimerling *et al.* submitted), we performed similar analyses on hexagons as the unit of analysis with qualitatively similar results.) In the 4-fold case, a hexagon tessellation to cover the icosahedron can only be constructed by connecting the centers of the triangle partition (figure 2 (*a*)). This is a so-called dual, or Voronoi, network corresponding to the triangle tessellation. In successive levels of the 4-fold hexagon hierarchy, each hexagon at a coarser level is composed of one whole and six half-hexagons from the next finer level. This results in an offset structure whereby no hexagon remains undivided over a minimum of two levels. This is a disadvantage in that aggregation and disaggregation of data require modelling the values in hexagons, either by smoothing or splitting, to change levels. On the other hand it is an advantage in avoiding the potential systematic bias in placement of a strictly congruent structure, such as a rectilinear quad-tree, that will divide an object located over cell intersections through all hierarchical levels (Nievergelt 1989).

For the 9-fold case, we illustrate in figure 2 (*b*) the construction of a hexagon tessellation by aggregation of triangles. (There is also a dual hexagon tessellation which, when combined with the tessellations formed by aggregation of triangles, creates a 3-fold hierarchy.) In successive levels of the 9-fold hexagon hierarchy each hexagon at a coarser level is composed of seven whole hexagons and six third-hexagons from the next lower level. This structure has the advantage of minimizing aggregation and disaggregation data modelling. On the other hand it lacks the offset property of the 4-fold hierarchy.

For either the 4-fold or 9-fold hierarchy, the hexagon tessellations over the entire sphere are always interrupted by either twelve pentagons or six squares located at the vertices of the icosahedron or octahedron, respectively, regardless of level in the hierarchy.

The principal criterion for selecting methods of mapping the partition from the geometric model to the surface of the sphere was the requirement that the method provide a one-to-one correspondence between points on the model of development, whether a plane, a polyhedron, or a sphere, and points on the surface of the sphere. For a map projection method this criterion implied that the extent of the planar triangle of the face of the geometric model be projected exactly to the corresponding extent of the spherical triangle of the geometric model. Many map projections, for example the Lambert equal area azimuthal, do not have this property (see White *et al.* 1992).

Using this criterion we implemented five methods of mapping the partition from the geometric model to the surface of the sphere. The first three methods map from the plane of an entire triangle of the geometric model to the sphere. The fourth method forms the partition by directly subdividing the spherical surface. The fifth method maps to the sphere from the vertices of successively higher order polyhedra formed by the recursive partition.

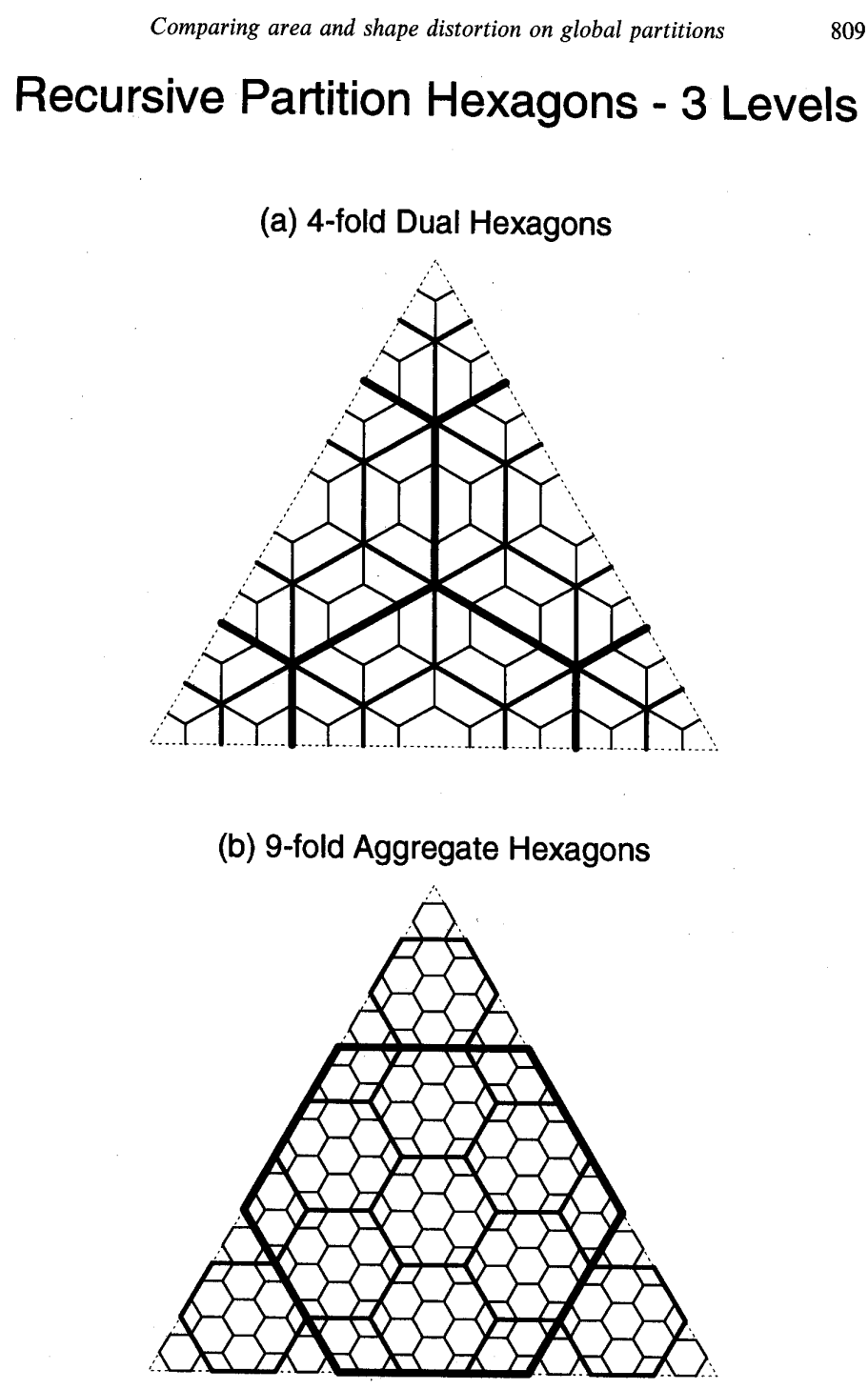

Figure 2. Hexagon tessellations resulting from recursive partitioning of a triangular face: (*a*) 'dual' hexagons from the 4-fold hierarchy; (*b*) 'aggregate' hexagons from the 9-fold hierarchy. The first three recursion levels are shown.

For the first three methods, we created the partitions in the plane and then projected the vertices to the sphere. The first of these methods was the Gnomonic azimuthal projection; the second was the Fuller Dymaxion projection (Fuller 1982, Gray 1994, 1995); and the third was the Snyder equal area polyhedral projection (Snyder 1992). The Gnomonic projection has the property that all straight lines in the plane correspond to great circle arcs on the sphere. Therefore we represented the edges of the partition cells on the surface of the sphere for this projection as great circle arcs. Since neither the Fuller nor the Snyder projection has this property, we used an approximation method to compute the edges on the sphere. At any level of recursion we projected not only the vertices of the triangle cells but also points along each edge computed in the plane from a $2^{(16\text{-recursion level})}$ subdivision of the edge. We calculated that this level of resolution of representation of the edges was sufficiently precise to compute our response variables to a precision of at least four significant digits for the highest level of recursion and at least six significant digits for all other levels.

The fourth method was to create the partition directly on the surface of the sphere. In this case, we used the same recursive rules with either the 4-fold or 9-fold increase in density. We started with the spherical triangle corresponding to a face of either the icosahedron or octahedron. This triangle's vertices are identical to those of the inscribed polyhedron and its edges are great circle arcs connecting these vertices. Then we bisected or trisected these edges (figure 3) depending on the change in density, as in the planar cases, and connected the nearest neighbour vertices with great circle arcs.

The final method was the polyhedral partition. In this method, the mapping from plane to sphere changed at each level of recursion. Each new vertex created by bisecting or trisecting an edge of a triangle was mapped to the surface of the sphere with the Gnomonic projection. This process was repeated recursively (figure 4). The edges of the cells of this partition on the sphere were then great circle arcs, since the Gnomonic projection always preserves the relation between lines in the plane and great circle arcs. For the 4-fold change in density, this method is equivalent to the direct spherical partition (figure 5).

We expected, of course, that the Snyder method would perform best in area distortion, by definition. Other expectations were that the Gnomonic mapping method would perform poorly, at least in area distortion, and that the Snyder method would likely sacrifice poor performance in shape distortion in achieving equal area.

We implemented the methods of partition for approximately four orders of magnitude difference in size of cells. For the 4-fold density ratio, we used recursion levels one through eight, and for the 9-fold density ratio, levels one through five (table 1).

3. Measures of performance

Analysis of distortion on map projections is commonly based on Tissot's theorem, leading to the concepts of scale, area, and angular distortion at a point on a projection (Robinson *et al.* 1995, Chapter 5, pp. 60–90). Angular distortion is sometimes used as a measure for shape distortion, but more explicit measures have also been developed (Kimerling *et al.* 1995). For our work, we chose to compute distortion measures based on properties of the cells of the recursive partitions as mapped to the sphere from the geometric model, either octahedron or icosahedron.

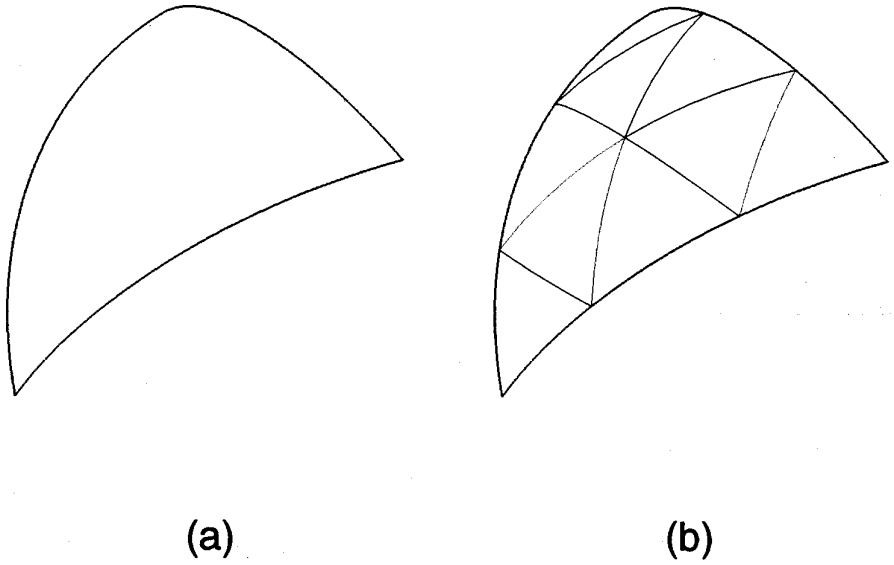

Figure 3. The Sphere method for projecting from the geometric model to the sphere. Starting with the initial model (icosahedron or octahedron) projected to the sphere, the spherical triangle is partitioned, using either the 4-fold or 9-fold density ratio, by either bisecting or trisecting each edge and connecting the new vertices with great circle arcs. In (*a*) the initial spherical triangular face is shown; in (*b*) the first level of the 9-fold partition is created by trisecting the edges and connecting nearest neighbour vertices.

We compared the performance of two general properties of the different methods of partition: area and shape distortion. For each general property we used several different measures. In order to make comparisons easier to interpret we used standardized measures. In each case of our analysis we started with a set of partition cells on the sphere, generated from one of the two geometric models, one of the two density ratios, one of the five methods for mapping the model to the sphere, and one of the eight or five levels of recursion, depending on density ratio.

The two direct measurements on partition cells that we used were the perimeter and area. The perimeter was calculated as the sum of great circle arc distances around the cell, including additional arcs introduced for the Fuller and Snyder projections to more accurately represent the boundary as mapped from the planar partition. The area of partition cells was calculated by Kimerling's (1984) formula for the spherical case.

For area measurements, we converted the actual areas to standardized areas for each level of recursion by dividing the actual areas by the values listed in table 1 to obtain areas relative to a unit value of 1.0. Since the Snyder projection is equal area, all area values at all levels are exactly equal to 1.0. No other mapping method had this property. One advantage of the standardization to unit areas is that measures

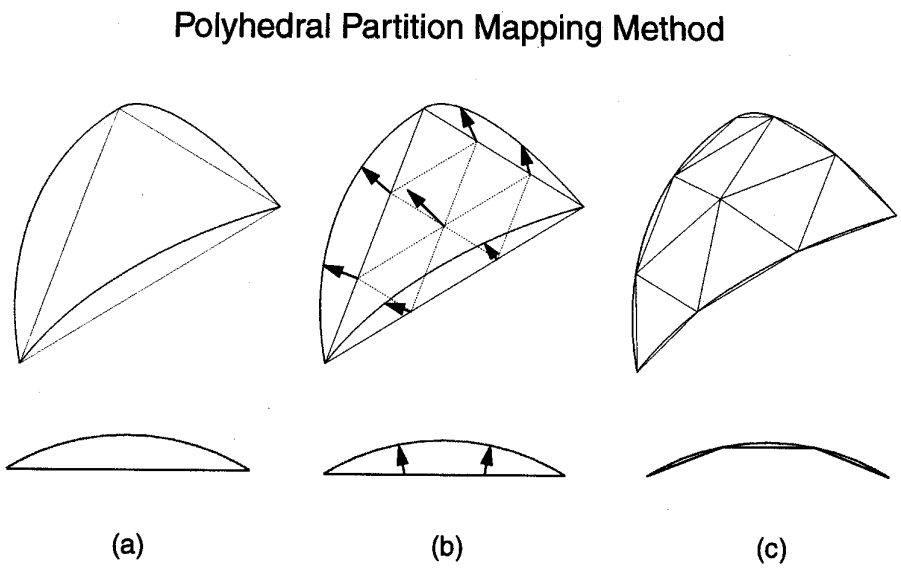

Figure 4. The Polyhedra method for projecting from the geometric model to the sphere. Starting with the initial model (icosahedron or octahedron) a face is successively subdivided, using either the 4-fold or 9-fold density ratio, to create successively higher order polyhedra using a Gnomonic projection of the edge bisection or trisection vertices to the surface of the sphere. In (*a*) the initial triangular face is shown with the corresponding spherical triangle determined by the vertices; in (*b*) the first level of the 9-fold partition is created in the plane of the face and each vertex is projected to the spherical triangle; in (*c*) the next level of polyhedron is created by connecting the projected vertices with chords. The first level polyhedron for the icosahedron has 180 faces (20×9).

of variation such as range and standard deviation are then relative to a standard unit and thus more directly comparable.

For shape measurements, we used a standardized perimeter to area ratio and called this 'compactness'. We defined this measure conceptually, for any cell, as the ratio of its perimeter to its area standardized by dividing this ratio by the highest value of compactness obtainable, that is, by the perimeter to area ratio of a spherical zone, bounded by a small circle, having the same area as the triangular cell. By a spherical zone we mean an area on the sphere contained within a spherical small circle. Computationally, this measure reduces to $\mathrm{sqrt}(4\pi a - a^2/r^2)/p$, where a is the cell area, p is the cell perimeter, and r is the radius of the sphere. The resulting values were then dimensionless numbers between 0 and 1.

We used five statistics of these two general types of measurements: range of area, standard deviation of area, range of compactness, standard deviation of compactness, and mean compactness. (Mean of area, as standardized, was always 1.0). Each statistic was computed for the population of all cells for each combination of a geometric model, mapping method, density ratio, and level of recursion, giving a total of $(2 \times 5 \times 8 = 80$, for 4-fold$) + (2 \times 5 \times 5 = 50$, for 9-fold$) = 130$ values of each statistic. (The Sphere and Polyhedra mapping methods are identical for the 4-fold density case.) Our analysis design is displayed in table 2 with the names that we will

Comparing Sphere and Polyhedra Methods

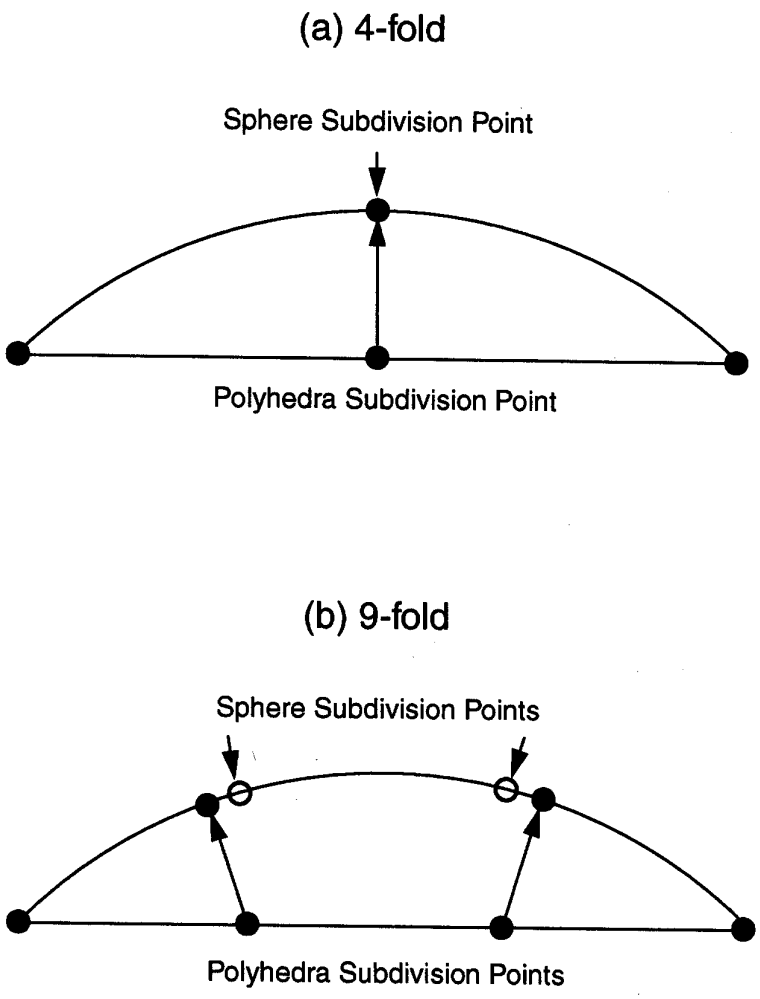

Figure 5. Comparison of the Sphere and Polyhedra mapping methods for one edge of one face: (*a*) for the 4-fold density ratio, the methods are identical; (*b*) for the 9-fold density ratio, the Sphere method creates equal arc lengths but the Polyhedra method projects the vertices of equal segment lengths on the edge to unequal arc lengths on the sphere.

use in subsequent discussion for the different components for each response measure and for each factor contributing to the response.

With these measurements we conducted sums of squares analyses to examine

Table 1. Partition characteristics for successive levels of recursion on a single face of the spherical octahedron and icosahedron. Areas are in square kilometers for an equal-area partition from a sphere with radius of 6370.9972 kilometre.

Level	Number of cells	Area per cell	
		Octahedron	Icosahedron
(*a*) 4-fold			
1	4	15939502.5	6375801.0
2	16	3984875.6	1593950.2
3	64	996218.9	398487.6
4	256	249054.7	99621.9
5	1024	62263.7	24905.5
6	4096	15565.9	6226.4
7	16384	3891.5	1556.6
8	65536	972.9	389.1
(*b*) 9-fold			
1	9	7084223.3	2833689.3
2	81	787135.9	314854.4
3	729	87459.5	34983.8
4	6561	9717.7	3887.1
5	59049	1079.7	431.9

Table 2. Components of the analysis design. Each response measure was computed for each combination of geometric model, mapping method, density ratio, and recursion level. Note that recursion levels 1–8 only apply to the 4-fold density ratio and recursion levels 1–5 only apply to the 9-fold density ratio.

Measures of response	Geometric models	Mapping methods	Density ratios	Recursion levels
Area range	Octahedron	Gnomonic	4-fold	1–8
Area std. dev.	Icosahedron	Fuller	9-fold	1–5
Compactness range		Snyder		
Compactness std. dev.		Sphere		
Compactness mean		Polyhedra		

components of variation, for which we further standardized the data. Sums of squares partitions of variation are computed using standard analysis of variance techniques in order to give a quantitative, relative comparision of the importance of individual factors and their interactions. Interpretation is based on the ratio of the mean square of effects (factors and their interactions) to mean square of residuals. To create comparable data for these analyses, we chose to standardize at one level of resolution as measured by mean size of partition cell. For this purpose, we selected the smallest cell size that made possible the estimation of the values of the statistics for all other cases (other combinations of geometric model and density ratio) by linearly interpolating between two adjacent values. Therefore we used recursion level 5 for the octahedron 9-fold density ratio with a cell size slightly greater than 1000 square kilometres (see table 1). We selected the smallest cell size that met the interpolation criterion both because the values in a recursion sequence tend toward an asymptote as the mean cell size decreases and because we expect most applications to use cell sizes at the smaller end of those we studied.

We also investigated the distribution of values and the spatial pattern of distortion, both in area and compactness, for combinations of mapping method and density ratio. In addition to histograms showing the distributions of values, we prepared maps representing, in the plane, the variation across a triangle of the icosahedron of both area and compactness values (see Clarke and Mulcahy 1995 for an alternative distortion mapping method). For these maps we used level 5 of the 4-fold density ratio and level 3 of the 9-fold density ratio. Rather than equal interval classes for these maps, we used quantiles to emphasize spatial pattern. We also computed and graphed correlograms showing the value of the autocorrelation of area and compactness measures as a function of distance separating cells. We used the same recursion levels for the correlograms as we did for the distortion maps. The units of distance on the correlograms are units of cell centre-to-centre distance. In this coordinate system, the length of a side of a 4-fold, level 5, base triangle is about 55 units and the distance from centre to vertex is about 33 units; for a 9-fold, level 3, base triangle, the side length is about 46 units and centre to vertex is about 27 units. We computed the correlograms for distances of 40 and 30 units, respectively, for the 4-fold, level 5, and the 9-fold, level 3 partitions.

4. Results

First we examined the performance of mapping methods by level of resolution for each of the five response measures (figure 6). Since the pattern of differences between methods as resolution was increased (cell size was decreased) was essentially identical for both geometrical models and for both density factors, we focus on the icosahedron 9-fold results.

Differences in range of area distortion illustrated a clear distinction among mapping methods as resolution was increased (figure 6(*a*)). Differences were less pronounced for the first level partition, but rapidly approached an asymptotic behaviour with the methods stabilizing at different levels of area range. The Gnomonic projection had approximately twice the range of area distortion (about 60% of the mean area) as that of the next largest, the Polyhedra method, followed in descending order by Sphere, Fuller, and Snyder. The Snyder projection had an area range of zero, of course, since it is an equal area mapping method. Standard deviation in area distortion (figure 6(*b*)) had the same order of performance in mapping method as did area range, with Gnomonic the highest and Snyder the lowest. (For the octahedron, although the differences between methods were similar, the maximum area range and the maximum standard deviation were more than twice as large as those for the icosahedron, being over 120% and 30%, respectively, both for the Gnomonic projection.)

For the compactness measures, the results were reversed with Snyder the highest both in range and standard deviation (figures 6(*c*) and 6(*d*)). Compared to Snyder the other methods were indistinguishable in range of compactness distortion (figure 6(*c*)). The Snyder performance apparently stabilized at a value much greater than any of the others. For the standard deviation of compactness distortion, however, the maximum values were at the first level of recursion (largest cell size) and then decreased in further levels of recursion for all methods. The Snyder performance was still distinctly greater than the others but may not have reached a minimum by level 5 of the 9-fold density ratio. The notable behaviour of the Snyder projection in stabilizing at a large compactness range but continuing to decrease in compactness standard deviation with increasing resolution can be partially understood by the

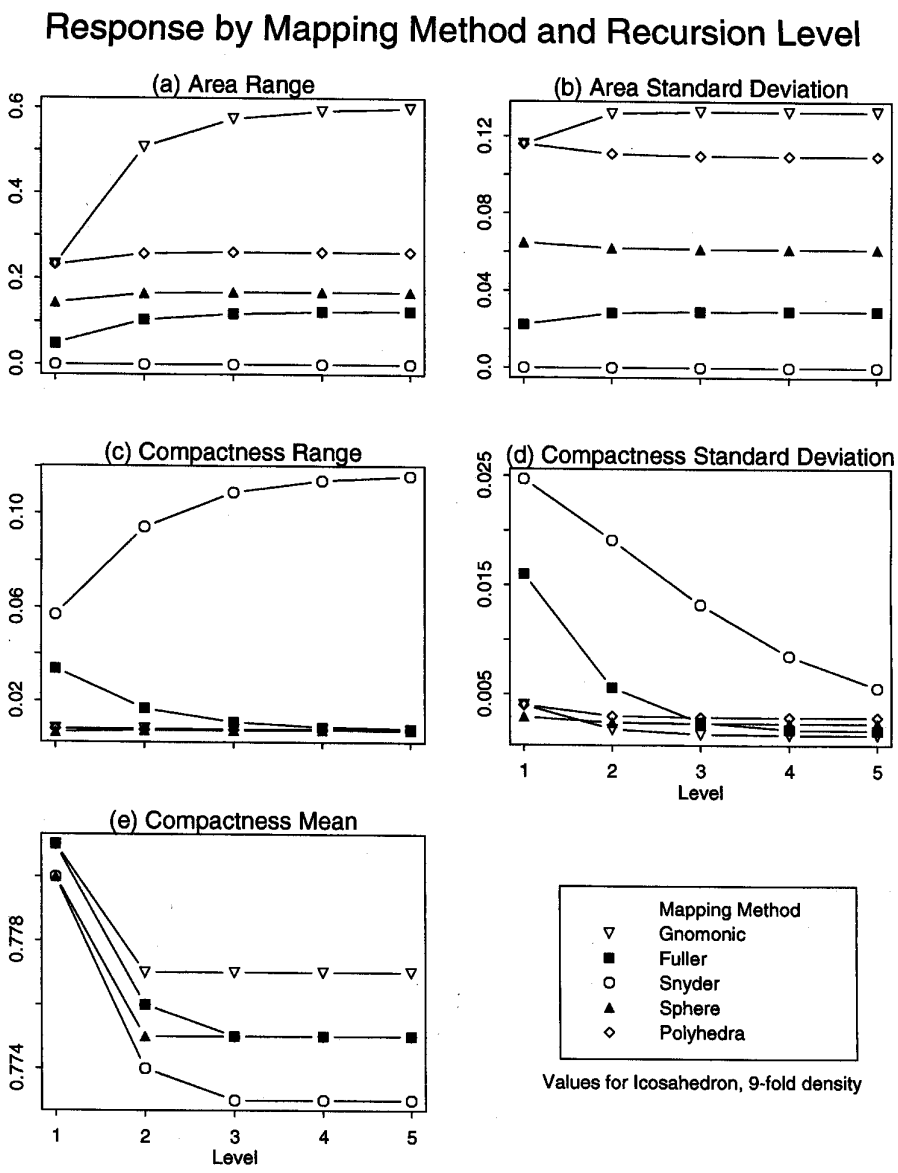

Figure 6. Graphs of the five statistics of the area and compactness response measurements shown for each mapping method as a sequence by recursion level. These results are for the icosahedron using the 9-fold density ratio.

maps of compactness values across a triangle of the icosahedron, to be discussed later. (For the octahedron, the maximum compactness variation measures were also more than twice as large as those for the icosahedron.)

Higher values of mean of compactness were closer to the most compact shape possible, and thus were preferred. The results of experiments for this measure were

somewhat surprising in that the Gnomonic projection had the best performance (highest values) and therefore, on average, the most compact cells. However, differences between methods were in the third decimal place indicating that for many applications the methods were not usefully distinguished. Also, none of the asymptotic values were greater than 78% of the most compact value possible, that of a spherical circle of the same area. (For the octahedron, the best performing method for mean of compactness was worse than the worst for the icosahedron, but differences between methods were also in the third decimal place.) The highest values for mean of compactness were at the first level partition for all methods; this result is understandable as the consequence of changing from a more rounded spherical triangle to a more nearly planar triangle as resolution increased.

The sums of squares analyses of variation sharpened our knowledge of the importance of different factors. By standardizing to the octahedron 9-fold density level 5, we developed a set of 20 values for each response measure, consisting of 5 methods times 2 models times 2 density factors (figure 7). For the Gnomonic and Fuller projections there was no apparent difference between density factors in any of the measures. The contrasting performance of the Snyder projection between area and compactness measures was also evident in figure 7, performing best in area but worst in compactness, except for compactness standard deviation in which the Polyhedra method was worst. Where there was a difference in density factor, the 9-fold values were consistently lower than the 4-fold, except for compactness standard deviation.

Another view of these results is a factor plot (figure 8), analogous to those used for analysis of variance (Chambers *et al.* 1992). These plots for each response measure show the means for the factors of geometric model, mapping method, and density ratio. The first indication of factor importance was that for the responses of area range, area standard deviation, and compactness range, mapping method accounted for more variation than geometric model, but that for the responses of compactness standard deviation and compactness mean, the results were reversed. In all cases variability due to density ratio was much less than that from the other two factors. This comparison of variation did not account for possible interactions between the factors. We investigated this with sums of squares analyses of variation.

We discuss in detail the sums of squares partition of variation in the area range response (table 3); analyses of the other response measures had similar results. Considering the main effects only (table 3(*a*)), the ratios of the mean square of the geometric model effect and the mapping method effect to the residual mean square were very high, but the corresponding ratio for the density ratio effect was over an order of magnitude lower. This confirmed the interpretation from the factor plot of this response (figure 8(*a*)). When we included all two-way interactions in the analysis (table 3(*b*)), the mean square ratio for the density ratio effect was higher than in the main-effects only analysis, but still over an order of magnitude less than either of the other main effects. The mean square of the effect of the interaction between geometric model and mapping method was about 14 times that of the residual mean square and this ratio was higher than that of the density ratio, suggesting some importance for this effect. This value was still about seven times lower than that of the lower value of the two factor effects themselves, however, implying that the interaction effect was substantially weaker than the main effects of these two factors. The other two interaction effects had even lower mean square ratios.

The histograms of the distributions of the area and compactness values for each

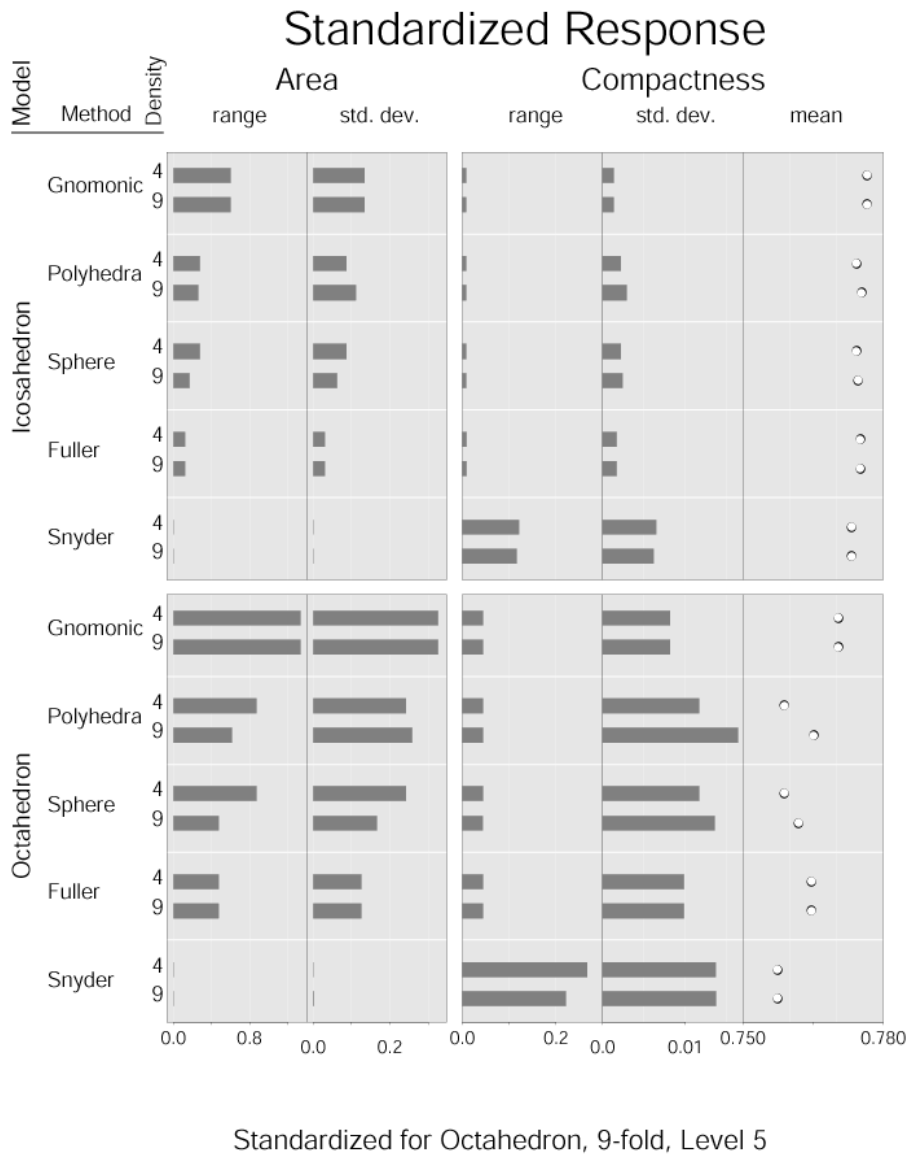

Figure 7. A row-labelled plot (Carr 1994) of the five statistics of the area and compactness response measurements as standardized for sums of squares analyses. These are shown for each geometric model, each mapping method, and each density ratio.

method (figure 9) showed distinct differences. The Snyder projection histogram for area (for the 4-fold density ratio) had only one bar for the single equal area value, but the histogram for the Snyder compactness values (for 4-fold) also had a surprising centrality of value. As figure 6(*c*) showed, however, the extreme values for the Snyder, though few in number, were substantially greater than for other methods. The Gnomonic and Fuller methods had continuous, unimodal histograms, while Sphere

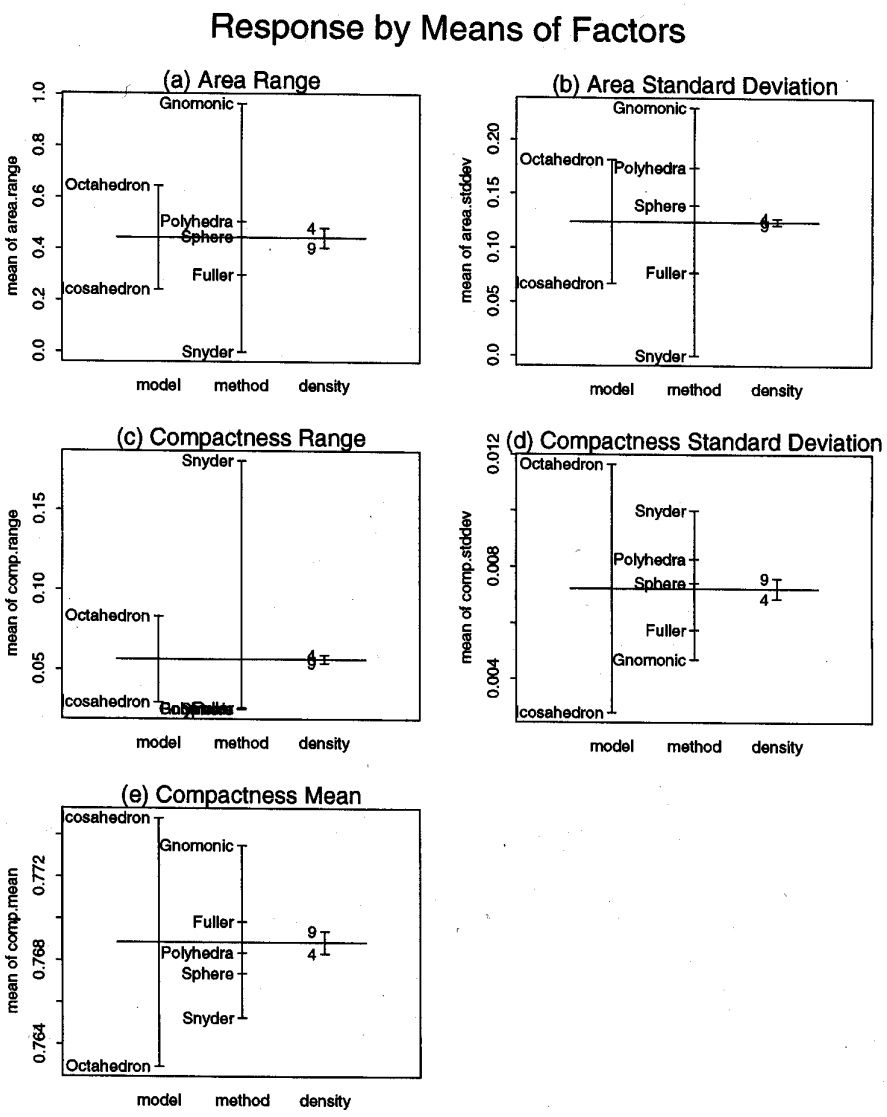

Figure 8. Graphs of the five statistics of the area and compactness response measurements, summarized by their means for the three factors of interest: geometric model, mapping method, and density ratio. For each of the five statistics, the geometric model values are the means of 10 standardized values (five mapping methods times two density ratios); mapping method values are the means of 4 standardized values (two geometric models times two density ratios); and density ratio values are the means of 10 standardized values (two geometric models times five mapping methods).

and Polyhedra had multimodal, discontinuous ones. Histograms of Gnomonic, Fuller, and Snyder for the 9-fold density ratio were essentially the same as the corresponding histograms for the 4-fold density ratio.

The maps of the spatial variation in the area and compactness values had

Table 3. Sums of squares analyses of variation results for area range response. The results are for two analyses: with and without two factor interactions. (Mean square ratios were computed with double [~14 digit] precision but rounded to one decimal place.)

	Degrees freedom	Sum of squares	Mean square	Mean square ratio
(a) Area range with main effects only				
Model	1	0.805	0.805	28.5
Method	4	1.976	0.494	17.5
Density	1	0.030	0.030	1.1
Residuals	13	0.368	0.028	
(b) Area range with two-way interactions				
Model	1	0.805	0.805	159.7
Method	4	1.976	0.494	98.0
Density	1	0.030	0.030	5.9
Model: method	4	0.283	0.071	14.0
Model: density	1	0.013	0.013	2.6
Method: density	4	0.052	0.013	2.6
Residuals	4	0.020	0.005	

fascinating patterns (figures 10–12). For the 4-fold density ratio, spatial variation in area (figure 10) had one of three patterns. The Snyder projection was homogeneous, being equal area. The Gnomonic and Fuller projections created partitions with a decrease in area per cell radially from the centre. The Sphere method created a pattern with an apparent fractal pattern. In compactness (figure 11), each method had a unique pattern of spatial variation. The Gnomonic had a general gradient of decrease in compactness per cell radially, as for the area measure, but with a more prominent 3-way symmetry. The Fuller pattern was dominated by abrupt change in first order neighbours. The Sphere pattern had a general gradient of decrease as with the Gnonomic, however the pattern followed the recursive block structure more closely.

The pattern of variation in compactness for Snyder had a strong 3-way symmetry about the angle bisectors along which the extreme values of Snyder lay. The evidence of this map, the Snyder compactness graph in figure 6, and the Snyder compactness histogram in figure 9, all helped in understanding the particular behaviour of this method. The mathematics of the projection constructed the equal area property across the full spherical triangle by distorting shape along the bisectors (Snyder 1992). Thus the map showed the extreme values located on the bisectors; the histogram displayed the large majority of values close to the mean with a small number of outliers (which were the values along the bisectors); and the graphs of standard deviation and range of compactness contrasted because the range contained the extreme values while the standard deviation gradually diminished as the number of cells along the bisectors became a smaller proportion of the total number of cells with increasing resolution of partition.

For the 9-fold density ratio, the Gnomonic, Fuller, and Snyder projections had patterns of area and compactness variation very similar to those for the 4-fold ratio. The patterns for Sphere and Polyhedra, however, were different (figure 12). Although each of these four patterns had the smallest values at the vertices and larger values toward the centre, the patterns had different, symmetric, and highly structured organization.

In a further examination of spatial structure with correlograms (figure 13), some

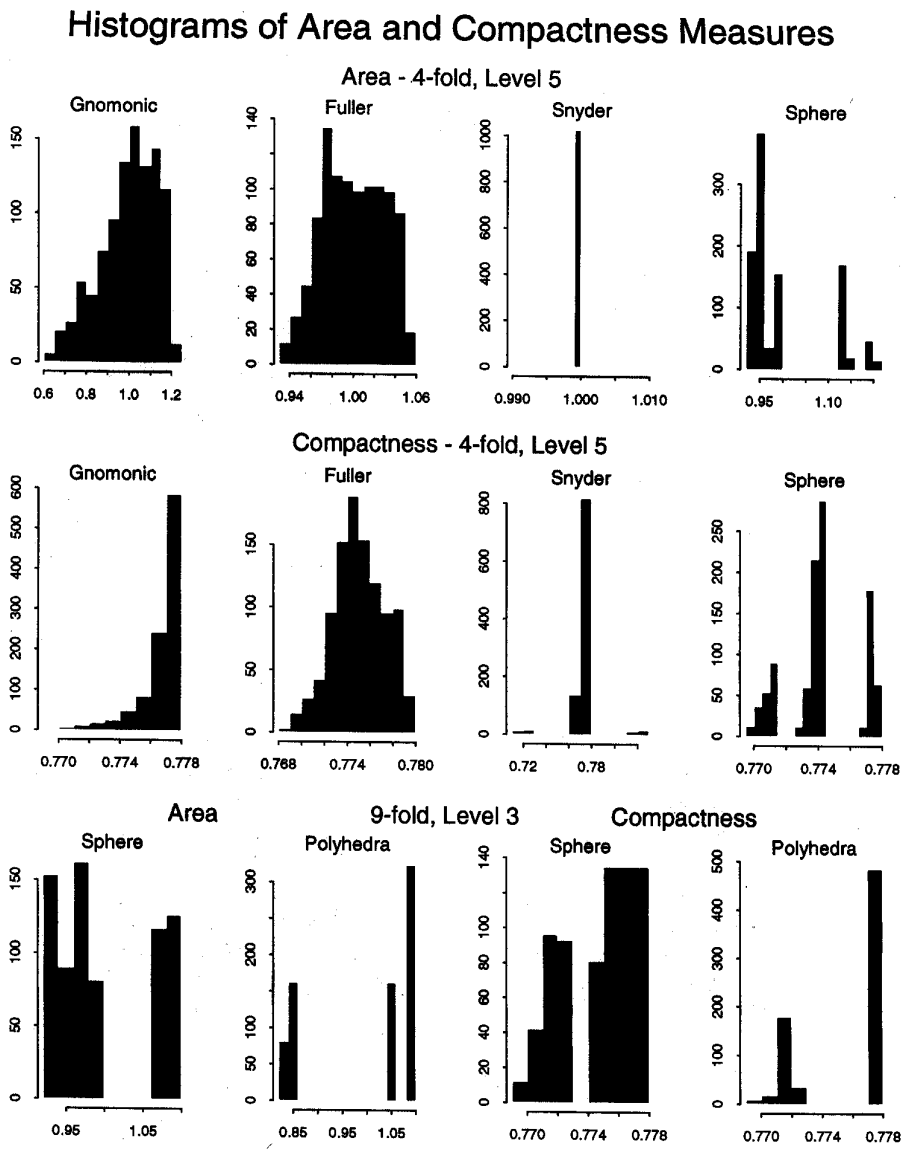

Figure 9. Histograms of the distributions of area and compactness measurements for different mapping methods and density ratios. These values are for the icosahedron partitions. Some combinations of mapping method and density ratio are not shown since they have similar patterns.

aspects of the mapped variation were confirmed. By definition, constant values yield autocorrelation values of zero, accounting for the Snyder area measure correlogram. The large alternation in values between adjacent cells in the compactness measure for Fuller was confirmed by the sawtooth shape of the autocorrelation function. The high negative autocorrelation of neighboring values along the angle bisectors of the

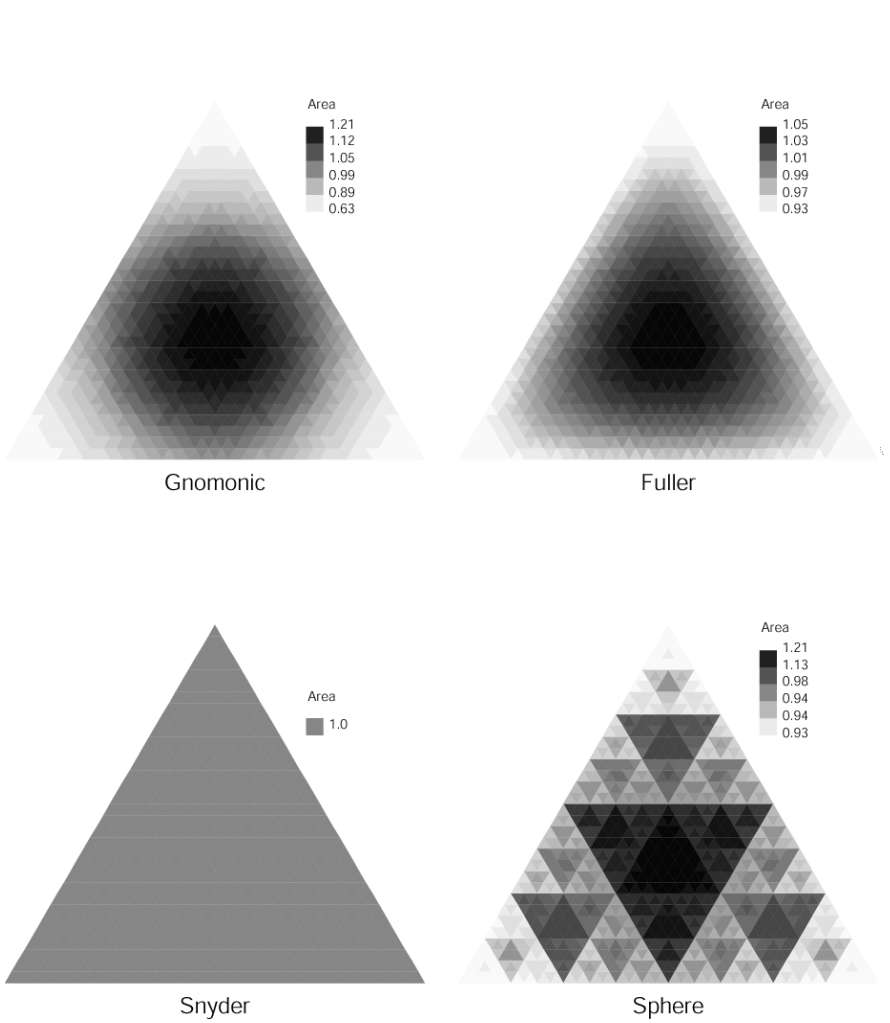

Figure 10. Maps of the spatial variation of area measurements for the Gnomonic, Fuller, Snyder, and Sphere mapping methods for the 4-fold density ratio.

compactness map for Snyder appeared in the negative first-lag autocorrelation value, in which these values along the angle bisectors were only partially offset by positive values in other parts of the map. The other correlograms had a common pattern of generally declining autocorrelation with distance. The Sphere and Polyhedra correlograms for both area and compactness had minor secondary peaks of increased values at distances of about 30 centre-to-centre distances for the 4-fold, level 5 partition and about 20 centre-to-centre distances for the 9-fold, level 3 partition.

5. Discussion

We have presented several complementary views of the distortion performance of different methods of partitioning the triangular faces of the icosahedron and

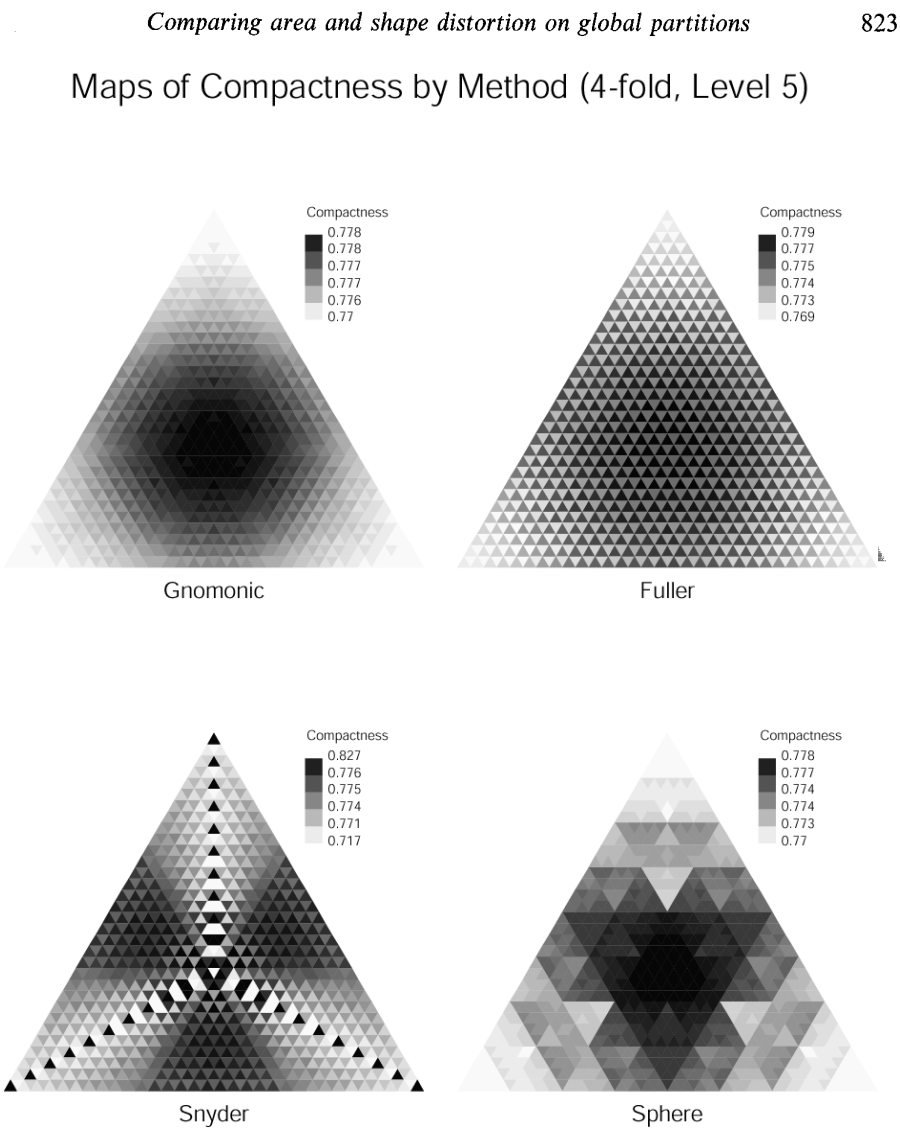

Figure 11. Maps of the spatial variation of compactness measurements for the Gnomonic, Fuller, Snyder, and Sphere mapping methods for the 4-fold density ratio.

octahedron (figures 6–13, table 3). These views taken together provided tools for evaluating the alternatives. Of the methods we analysed, only the Snyder projection had the equal area property. For applications that require this property, our analyses demonstrated the cost in considerable shape distortion compared to other methods. For applications that could confine their study area to between the angle bisectors, the cost would not be great. However, these applications are not the most likely to use a global system.

If exact equal area is not required, other factors may be considered. The best performance in shape distortion, both in variability and in mean value, appeared to be from the Gnomonic projection (figures 6 and 7). We conjecture that this is because

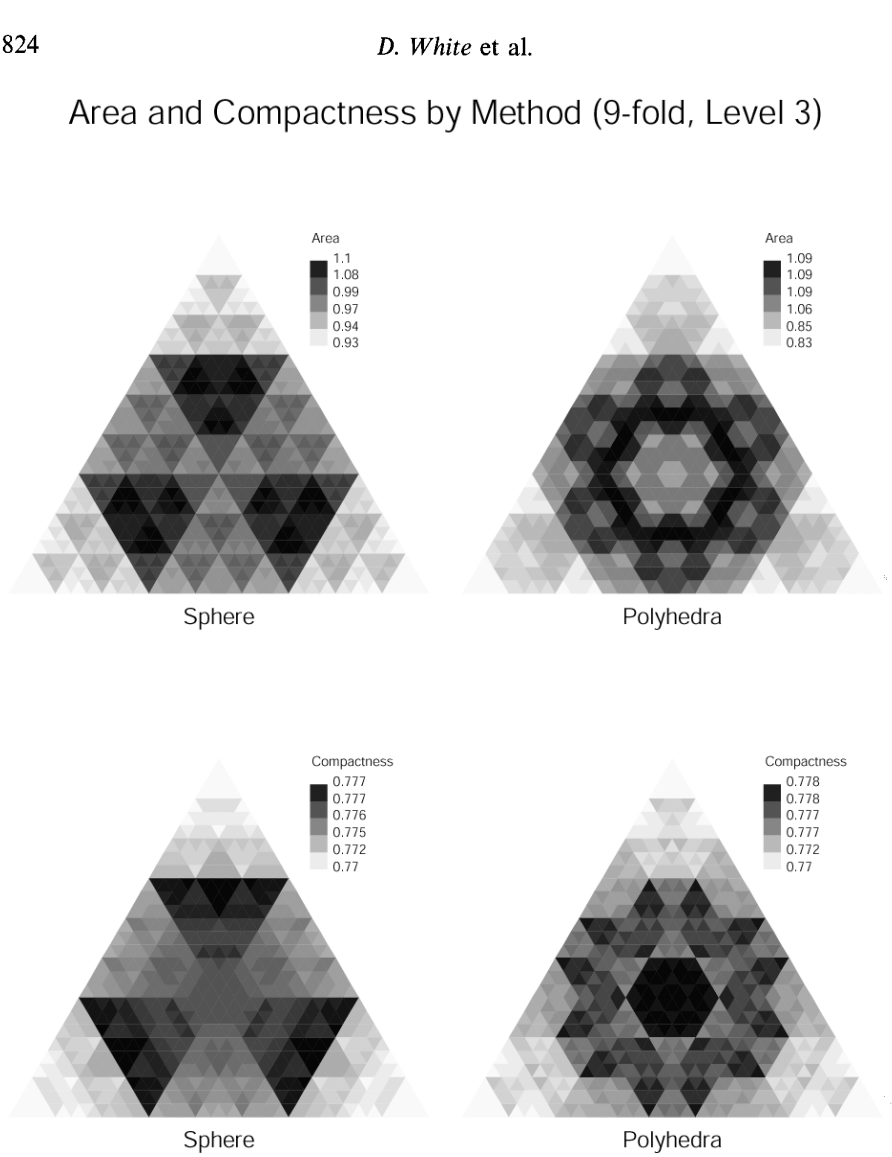

Figure 12. Maps of the spatial variation of area and compactness measurements for the Sphere and Polyhedra mapping methods for the 9-fold density ratio.

the cell edges are always great circle arcs, minimizing shape deviations due to edge curvature. Another criterion for judging performance could be balance between area and shape distortion, under which Fuller or Sphere could be candidates. For distinguishing between these two mapping methods, the histograms and maps provide the best evidence. Fuller had a generally smoother distribution of values in both area and compactness whereas Sphere had multi-modal distributions and highly structured spatial variability.

The contrast between the 4-fold and 9-fold density ratios was not an important factor in distortion performance as indicated by the factor plots (figure 8) and the sums of squares analyses (table 3). Choosing between these may be better determined

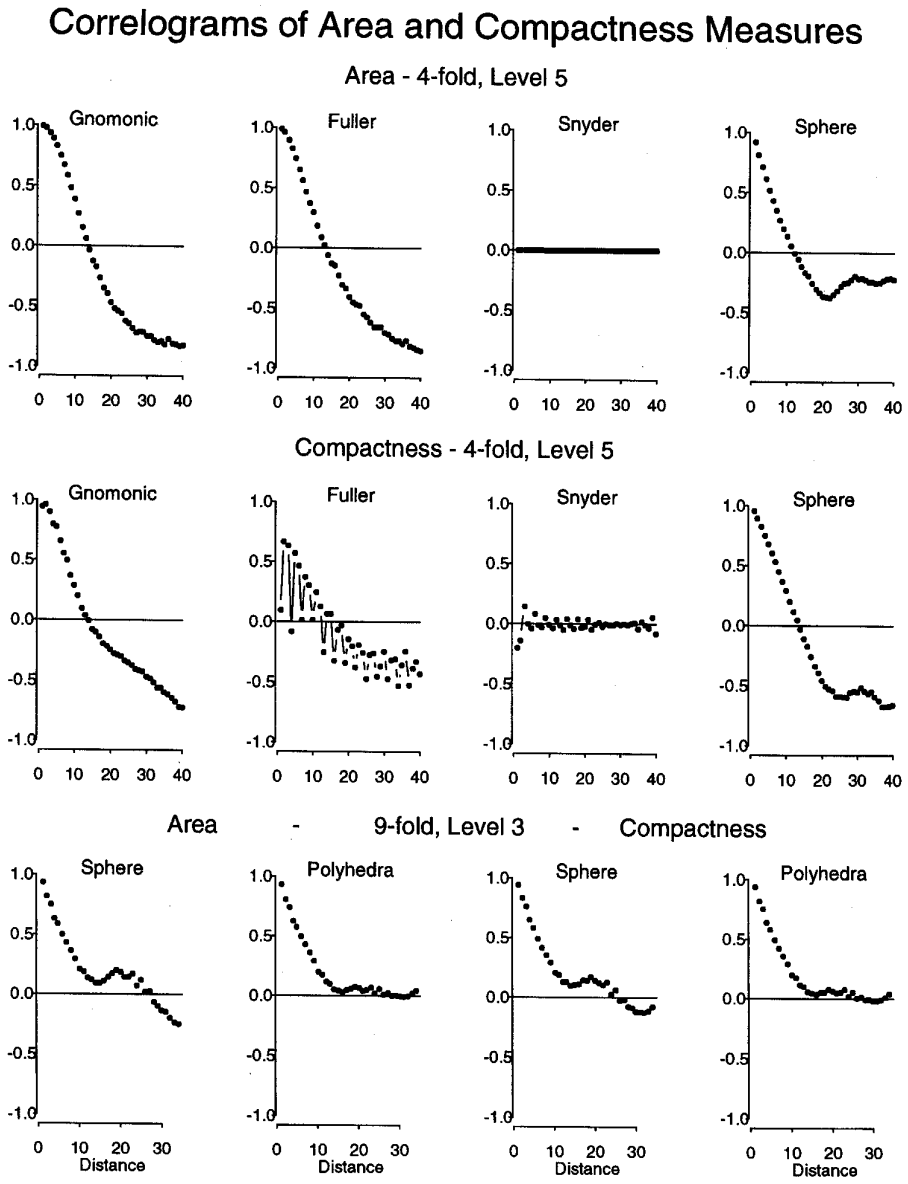

Figure 13. Correlograms of the area and compactness measurements for different mapping methods and density ratios. These values are for the icosahedron partitions. Some combinations of mapping method and density ratio are not shown since they have similar patterns.

by other criteria, for example, scaling considerations or data structure development. The 4-fold ratio provides a finer scale gradient than the 9-fold for choosing cell size; however, the 9-fold can be augmented to form a 3-fold density ratio system, consequently having finer gradations than the 4-fold. The 4-fold system could adopt the

data structure technology of quad-trees (Fekete and Treinish 1990, Lugo and Clarke 1995); however, 9-fold or 3-fold hierarchies could be constructed analogously with ternary or non-anary trees. One other criterion is object integrity over changes in recursion level; we discussed this under advantages for each density ratio.

Our results showed clear differences, as expected, between using the icosahedron or octahedron as an initial geometric model. In every measure of performance the icosahedron scored better than the octahedron. Preference for the octahedron therefore would have to rely on other criteria. One of these could be ease of orientation, since the octants can be aligned with major divisions in the graticule (Gasson 1983). Another might be minimizing singularities (six vertices rather than twelve).

This analysis investigated the distortion characteristics of the triangular cells of recursive partitions. We have also compared in a more recent study (Kimerling *et al.* 1997) distortion on hexagon cells for the Snyder and Fuller methods with results that are qualitatively similar to those in this study.

The factorial design of our analysis and the complementary statistical and graphical tools allowed for comparisons between alternative methods of constructing spherical tessellations. We have looked at a subset of the many possible types of these tessellations and used only two general types of performance measurements. For example, minimizing distortion may not be the only goal of a global grid partition system. Other relevant goals could include ease of constructing neighbourhoods of cells, ease of navigating along routes, and ease of performing other analytical tasks such as cartographic generalization. We also did not examine the placement or orientation of polyhedral models with respect to fixed points on the earth in order to minimize distortion for land areas, for example. Future analyses could include tessellations based on whole-earth map projections, for example, rather than only polyhedral systems, and could include other measurements of performance such as variability in centre point distances and the computational complexity of retrieval and calculation tasks using the partition structure.

Acknowledgments

We would like to acknowledge support from cooperative agreement CR 821672 between the US Environmental Protection Agency and Oregon State University and helpful suggestions during the course of this research from Anthony Olsen of US EPA and N. Scott Urquhart of Oregon State University. Pip Courbois and Dan Carr helped with the preparation of figure 7. Robert Gray and several reviewers made helpful comments. This research has not been officially reviewed by US EPA and no endorsement should be inferred.

References

CARR, D. B., 1994, Converting tables to plots. Technical Report 101, Center for Computational Statistics, George Mason University, Fairfax, VA.

CHAMBERS, J. M., FREENY, A. E., and HEIBERGER, R. M, 1992, Analysis of variance; designed experiments. In *Statistical Models in S*, edited by J. M. Chambers and T. J. Hastie (Pacific Grove, CA: Wadsworth & Brooks), pp. 145–193.

CLARKE, K. C., and MULCAHY, K. A., 1995, Distortion on the Interrupted Modified Collignon Projection. In *Proceedings, GIS/LIS '95, Annual Conference and Exposition* (Charlotte, NC: Urban and Regional Information Systems Association), pp. 175–181.

DUTTON, G., 1988, Modeling locational uncertainty via hierarchical tessellation. In *Accuracy of Spatial Databases*, edited by M. Goodchild and S. Gopal (New York, NY: Taylor & Francis), pp. 123–140.

DUTTON, G., 1996, Improving locational specificity of map data—a multi-resolution,

metadata—driven approach and notation. *International Journal of Geographical Information Systems*, **10**, 253–268.

FULLER, R. B., 1982, *Synergetics* (New York, NY: MacMillan).

FEKETE, G., and TREINISH, L. A., 1990, Sphere quadtrees: a new data structure to support the visualization of spherically distributed data. In *Proceedings of the SPIE, Extracting Meaning from Complex Data: Processing, Display, Interaction, Volume 1259*, edited by E. J. Farrell (Bellingham, WA: The International Society for Optical Engineering), pp. 242–253.

GASSON, P. C., 1983, *Geometry of spatial forms* (Chichester: Ellis Horwood Limited).

GOODCHILD, M. F., and YANG SHIREN, 1992, A hierarchical spatial data structure for global geographic information systems. *Computer Vision, Graphics and Image Processing*, **54**, 31–44.

GRAY, R. W., 1994, Fuller's Dymaxion ™ map. *Cartography and Geographic Information Systems*, **21**, 243–246.

GRAY, R. W., 1995, Exact transformation equations for Fuller's world map. *Cartographica*, **32**, 17–25.

KIMERLING, A. J., 1984, Area computation from geodetic coordinates on the spheroid. *Surveying and Mapping*, **44**, 343–351.

KIMERLING, A. J., OVERTON, W. S., and WHITE, D., 1995, Statistical comparision of map projection distortions within irregular areas. *Cartography and Geographic Information Systems*, **22**, 205–221.

KIMERLING, A. J., SAHR, K., and WHITE, D., 1997, Global scale data model comparison. In *Proceedings, Auto-Carto 13* (Bethesda, MD: American Society for Photogrammetry and Remote Sensing), pp. 357–366.

LUGO, J. A., and CLARKE, K. C., 1995, Implementation of triangulated quadtree sequencing for a global relief data structure. In *Proceedings, Auto-Carto 12* (Bethesda: American Congress of Surveying and Mapping), pp. 147–156.

NIEVERGELT, J., 1989., 7 ± 2 criteria for assessing and comparing spatial data structures. In *Design and Implementation of Large Spatial Databases*, edited by A. Buchmann, O. Günther, T. R. Smith, and Y. -F. Wang, Lecture Notes in Computer Science 409 (Berlin: Springer-Verlag), pp. 3–27.

POPKO, E., 1968, *Geodesics* (Detroit, MI: University of Detroit Press).

ROBINSON, A. H., MORRISON, J. L., MUEHRCKE, P. C., KIMERLING, A. J., and GUPTILL, S. C., 1995, *Elements of Cartography, Sixth Edition*, (New York, NY: John Wiley & Sons).

SNYDER, J. P., 1992, An equal-area map projection for polyhedral globes. *Cartographica*, **29**, 10–21.

WHITE, D., KIMERLING, A. J., and OVERTON, W. S., 1992, Cartographic and geometric components of a global sampling design for environmental monitoring. *Cartography and Geographic Information Systems*, **19**, 5–22.